Chemical Engineering Journal 285 (2016) 286–292

Contents lists available at ScienceDirect

Chemical Engineering Journal

journal homepage: www.elsevier.com/locate/cej

Continuous microfluidic synthesis and functionalization of gold nanorods

Laura Uson [a], Victor Sebastian [a,b], Manuel Arruebo [a,b,*], Jesus Santamaria [a,b,*]

[a] Institute of Nanoscience of Aragon (INA) and Department of Chemical and Environmental Engineering, University of Zaragoza, C/Mariano Esquillor, s/n, I+D+i Building, 50018 Zaragoza, Spain
[b] Networking Research Center on Bioengineering, Biomaterials and Nanomedicine, CIBER-BBN, 28029 Madrid, Spain

HIGHLIGHTS

- The continuous synthesis and functionalization of gold nanorods is achieved.
- A 100-fold reduction in PEG consumption is possible by using microfluidics.
- The system facilitates tuning the concentration of halides to modify the nanorods.

GRAPHICAL ABSTRACT

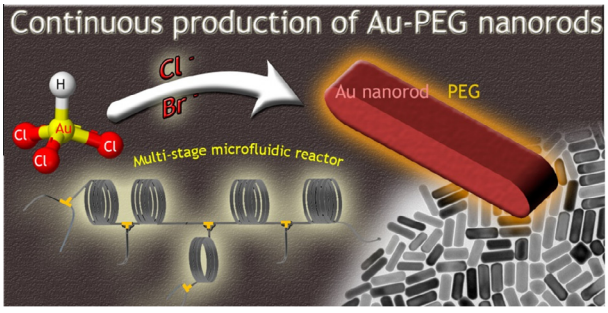

ARTICLE INFO

Article history:
Received 25 June 2015
Received in revised form 15 September 2015
Accepted 29 September 2015
Available online 9 October 2015

Keywords:
Microfluidics
Gold nanorods
PEG
Plasmonics

ABSTRACT

A microfluidic platform with multiple reactant additions has been used for the continuous, unseeded synthesis of gold nanorods. This system allows separate control of the seed forming and nanorod growing stages, increasing reproducibility and reducing undesired effects related to a poor control of the seed aging stage. Also, on-stream surface functionalization with poly(ethylene glycol)-methyl ether thiol (SH-PEG) has been performed, allowing a 100-fold reduction in the consumption of this reactant compared to the amounts used in a conventional batch reactor. The system also facilitates tuning the concentration of halide anions (Cl^- and Br^-) that are used to modify the aspect ratio of the resulting rods.

1. Introduction

During crystallization, when the concentration of precursors in the solvent exceeds its equilibrium solubility or the temperature decreases below a phase change, new nuclei are formed. A successful separation of nucleation and growth processes during nanoparticle crystallization is critical to control the size, shape and composition of the resulting nanomaterials. Even though both events may still occur simultaneously, in conventional batch reactors an effective approach to limit additional nucleation events during the growth stage is to reduce the reagents concentration below the critical supersaturation level [1]. Alternative procedures to promote crystal growth while minimizing new nucleation events make use of the different temperature dependence of nucleation and growth kinetics [2] or, in the case of metallic nanoparticle synthesis, of weaker reducing agents during the growth step [3]. The particle size distribution can also be narrowed

* Corresponding authors at: Institute of Nanoscience of Aragon (INA) and Department of Chemical and Environmental Engineering, University of Zaragoza, C/Mariano Esquillor, s/n, I+D+i Building, 50018 Zaragoza, Spain.
E-mail addresses: arruebom@unizar.es (M. Arruebo), jesus.santamaria@unizar.es (J. Santamaria).

http://dx.doi.org/10.1016/j.cej.2015.09.103
1385-8947/

through additional processing tools. Thus, polydisperse seeds from a burst La Mer-type nucleation can eventually reshape or grow rendering nearly monodisperse suspensions by Oswald [4] or digestive ripening processes [5] and by the competition between coalescence and stabilization with the capping agents used during synthesis [6,7].

Microfluidic reactors provide a different path for the separation of nucleation and growth by having, in the same synthesis platform, two distinct zones for each of these processes. High heat transfer rates are characteristic of microfluidic processing, due to their large interfacial surface area-to-volume ratio, with heat exchange coefficients that are up to one order of magnitude higher than those in conventional batch reactors [8]. Because of the fast heating and quenching rates, large temperature gradients are easily achievable, and the different temperature dependence of nucleation and growth kinetics can be fully exploited.

When microreactors are used for nanoparticle synthesis, molecular diffusion governs reactant mixing since these reactors operate in the laminar flow regime. When molecular diffusion is sufficiently fast, radial concentration gradients are minimized, rendering monodisperse nanoparticles [9]. In addition, in sharp contrast to batch reactors scale up is straightforward by numbering up (arraying parallel microreactors). In this regard, by using parallel operation of microreactors a combinatorial synthesis of nanomaterials with exquisite kinetic control has been demonstrated [10]. Examples of successful scaled up synthesis processes include high-throughput production of nanoparticles (polymeric, lipidic, inorganic, polyplexes, etc. functionalized or not) up to 3 Kg/day using microfluidic jet mixers [11], and flow focusing systems using 3D flash flow microreactors to produce polymeric nanoparticles at rates as high as 12.9 g/h [12]. On stream real-time monitoring of the quality of continuously produced nanomaterials is also a great advantage when using microfluidic platforms [13]. Downstream control systems had been successfully implemented with feedback from online monitoring to drive the system towards a product with desired properties [14]. Also, microfluidic systems are ideally suited to implement additional reaction stages to provide the final nanoparticles with multiple features [15].

The use of microfluidic reactors for nanoparticle synthesis extends to materials of any nature including ceramics [16,17], semiconductor nanocrystals [18,19], metals [20], magnetic oxides [21], polymers [12], micelles [22], liposomes [23], niosomes [24], MOFs [25], and anisotropic materials [26,27]. Anisotropy is often desirable because it enables specific size-dependent properties. This is the case of the transverse and longitudinal modes of surface plasmon oscillations in the case of gold nanorods. This property make them useful in a variety of applications including biosensing, Raman scattering of adsorbed molecules, catalysis, photothermal therapy, optical labeling, medical imaging, drug and gene delivery, etc. In addition, the frequency of the longitudinal band can be red-shifted from the VIS to the NIR range by increasing the aspect ratio of the rods. High aspect-ratio rods are usually synthesized using hydrophobic co-surfactants as stabilizers [28] or using hydrophobic reducing agents which are inserted into the hydrophobic part of the double layer of the hexadecyltrimethylammonium bromide (CTABr) to again stabilize the rod-shaped template that CTABr provides [29]. In those nanomaterials additional higher order modes of surface plasmon oscillations such as quadrupole and sextupole resonances are possible, although they require a particular light incident angle and polarization state.

Both, seeded and un-seeded methods have been used for the synthesis of gold nanorods. In the seeded-growth method a reducing agent is used to form in a first stage Au(0) nanoseeds from a gold precursor. These seeds are induced to grow into gold nanorods in a second stage by using molecules (usually cationic surfactants) that adsorb preferentially on specific crystal facets showing high surface energies (i.e., [1 1 0]). Often, small concentrations of additional ions (such as silver [30] or halides [31]) are used as surface passivation components in a structure-directing role that enables control on the nanorod aspect ratio [32]. The seedless methods involve the consecutive formation of seeds and rods without having two separate stages by performing a fast reduction (adding a strong reducer instead of seeds) and a slow rod growth in the same reactor; however seedless methods are very sensitive to synthesis parameters and usually produce rods with reduced aspect ratio [33,34]. Separately prepared gold seeds have been used in millifluidic reactors to reach gram scale production of gold nanorods [13]. Also, the same reactor was used to prepare the rods following the seedless method demonstrating the robustness of those systems. Sequential microfluidic reactors using segmented flow have been used to obtain gold nanorods by first synthesizing gold seeds that are then grown into rods [33]. However in this case the use of immiscible liquids for the segmented flow has the disadvantage of requiring a high efficiency downstream liquid separator or, alternatively, accepting the reduction in the speed of the process if conventional decantation is used. The high-throughput millifluidic seedless system developed by Lohse et al. [13] started to produce gold nanorods after 6 min residence time being completely formed after 15 min.

In this work, we present a simple method for microfluidic seedless synthesis of gold nanorods. We show, as a novelty compared with the previous works, that this can be achieved with similar residence times without the need of using segmented flow and, in addition a continuous surface PEGylation can be added on the same microfluidic platform. Surface PEGylation reduces the cytotoxicity of CTABr-capped gold nanorods [35] and therefore a process that allows continuous seedless synthesis and surface functionalization of gold nanorods has a clear interest in the biomedical field.

2. Experimental section

Hexadecyltrimethylammonium bromide (CTABr) (Sigma, 98%), gold(III) chloride solution (Sigma, 30 wt.%), sodium borohydride (Sigma, 98%), silver Nitrate, L-ascorbic acid (Sigma, 99%), hydrogen tetrabromoaurate(III) hydrate (Sigma), 5-bromosalicylic acid (Sigma, 90%), poly(ethylene glycol) methyl ether thiol (Sigma, Mn 800) were used as received without further purification.

Fig. 1 shows the experimental microfluidic platform used in this work. The microfluidic platform is divided in four stages connected by PTFE microtubing that allows visual access to the gold transformations along the different stages of the system: (1) Gold precursor activation, where Au(III) is reduced to Au(I) by ascorbic acid [36]; (2) Au seeds formation through the fast reduction of Au(III) to Au(0) by $NaBH_4$; (3) Au nanorods formation, following the seed-mediated growth and (4) Au nanorods pegylation. The corresponding residence times of each stage are described in Fig. 1. The system was fed through a set of syringe pumps (Harvard apparatus PHD ULTRA™ CP 4400) and interfaced with PEEK-based Y-shaped junctions using PTFE tubing (I.D. = 1.016 mm) with the appropriate length to keep the desired residence times. Fig. 1 compiles the chemical composition of the solutions used in the inlets of the microfluidic system, as well as their corresponding flow rates. Finally, Thiol-PEGylation was carried out by adapting the protocol developed by Maltzahn et al. [37] for batch systems into a continuous fashion.

To analyze the influence of the bromide ions in the synthesis of the gold nanorods two modifications were studied, either adding Hydrogen tetrabromoaurate(III) hydrate instead of Gold(III) chloride solution as gold precursor, or adding directly 5-bromosalicylic acid to obtain a 88 mM solution in the Inlet 1.

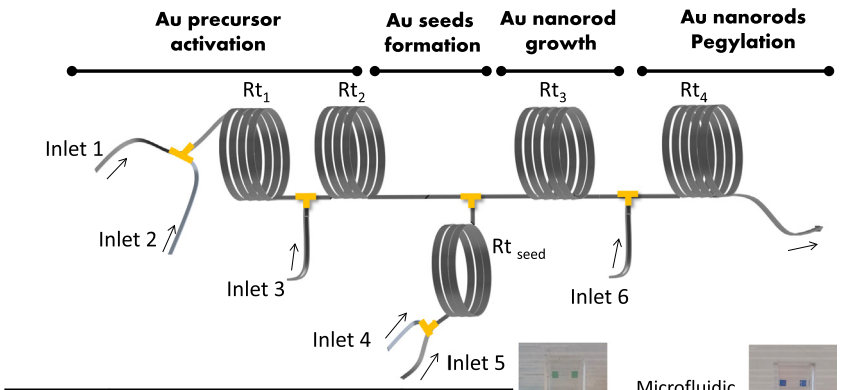

	Reagents	F (mL/h)
Inlet 1	- CTABr (190 mM) - $AgNO_3$ (0,19 mM) (* 5-Bromosalicylic Acid, 88mM)	5.85
Inlet 2	- $HAuCl_4$, (0.94 mM) (*/ $HAuBr_4$, 0,94 mM)	5.85
Inlet 3	- Ascorbic Acid (34.7 mM)	0.67
Inlet 4	- $HAuCl_4$ (0.45 mM)	0.62
Inlet 5	- $NaBH_4$ (10.7 mM) - CTABr (178.6 mM)	0.62
Inlet 6	- Poly(ethylene glycol) methyl ether thiol (1.13 μM)	3.4

* Optional Reagent added according to experimental section

Residence time Zone	Time, min
Rt_1	6
Rt_2	6
Rt_3	10
Rt_4	10
Rt_{seeds}	2
$Rt_{microfluidic\ system}$	32

Fig. 1. Experimental set-up for the seedless synthesis and continuous PEGylation of gold nanorods. The flow rates and compositions are given for the different feed streams, as well as residence times corresponding to each reactor zone.

In the first approach (replacement of chlorine for bromide ions in the gold precursor) Inlet 2 was a solution of $HAuBr_4$ (0.94 mM).

Particle morphology and size distribution have been determined in the Advanced Microscopy Laboratory (LMA) of our Institute by using a T20-FEI Tecnai thermoionic transmission electron microscopy (TEM) operated at 200 kV with a LaB6 electron source fitted with a "SuperTwin®" objective lens allowing a point-to-point resolution of 2.4 Å. Aberration corrected scanning transmission electron microscopy (Cs-corrected STEM) images were acquired using a high angle annular dark field detector in a FEI XFEG TITAN electron microscope operated at 300 kV equipped with a CETCOR Cs-probe corrector from CEOS Company allowing formation of an electron probe of 0.08 nm. Elemental analysis was carried out with an EDS (EDAX) detector which allows performing EDS experiments in the scanning mode. At least 200 particles were measured to evaluate the mean diameter of the particles and aspect ratio (length/width) distribution. To prepare the sample for TEM observation, the nanoparticle-based suspension was diluted with Milli-Q water and sonicated for 30 s before the casting of 5 μL on a holey carbon supported TEM grid. A 7 wt.% solution of phosphotungstic acid was used as a negative stain to allow electron observation of the PEG coating [15].

3. Results and discussion

To illustrate the drawbacks of the conventional batch synthesis, different batch-prepared seeds with different aging times were used to generate gold nanorods (Fig. 2). Depending on the aging time and therefore on the size of the seeds, the resulting characteristic localized surface plasmon resonance absorption peaks varied significantly (see Fig. 2a). The longer the aging time the larger the size of the resulting seeds (see Fig. 2b and d) and therefore, for seeds prepared after 125 min of aging a characteristic absorption peak starting at 520 nm was observed. Smaller seeds (<3 nm) obtained at short aging times did not show any absorption due to quantum size effects related to the low electron density in the conduction band in agreement with the literature [38,39]. Larger seeds produced rods with a lower aspect ratio (see Fig. 2d and f; the resulting aspect ratios were 8.6 and 5.6 for seeds aged during 2 min (see Fig. 2c) and 125 min respectively) in agreement with previous results [36]. The main advantage of microfluidic reactors is that, seed formation and aging on the one hand, and nanorod growth on the other, can be clearly separated carried out in a continuous fashion, with an exquisite control of residence times at each stage. This allows to fine tune the seed formation process, avoiding any uncontrolled seed-aging dependence. Microfluidic reactors allow controlling precisely the size of the seeds and consequently the epitaxial growth of gold nanorods can be tuned in order to obtain a desired aspect ratio. In the microfluidic channel the ascorbic acid used as mild reductant forms Au(0) nanoseeds in first stage from the gold precursor. During the heterogeneous crystallization these seeds are induced to grow into gold nanorods in a second stage by using CTABr and silver (and also halides) which adsorb preferentially on specific crystal facets with high surface energies rendering gold nanorods with specific aspect ratios.

Due to the laminar flow regime used, mixing is only attributable to molecular diffusion. We can roughly estimate the characteristic mixing time based on Fick's law as $Tmix = dt^2/4D$, where dt is the tube diameter and D is the diffusion coefficient. Considering a nominal diffusion coefficient of 10^{-9} m^2 s^{-1}, the calculated Tmix is approximately 4 min. It is necessary to highlight that this should be the worst case scenario since this calculation does not take into account the effect of the chemical reaction occurring when the gold precursor and the reducing agent (two reactive streams) are mixed. Consequently, under the current conditions the mixing time is under the residence time required to grow the gold nanorods (10 min) which guarantees an appropriate mixing.

Nanoparticle size dispersion in the microchannel and wide residence time distributions, due to the parabolic flow profile, are reduced thanks to the use of low flow rates. When a microfluidic

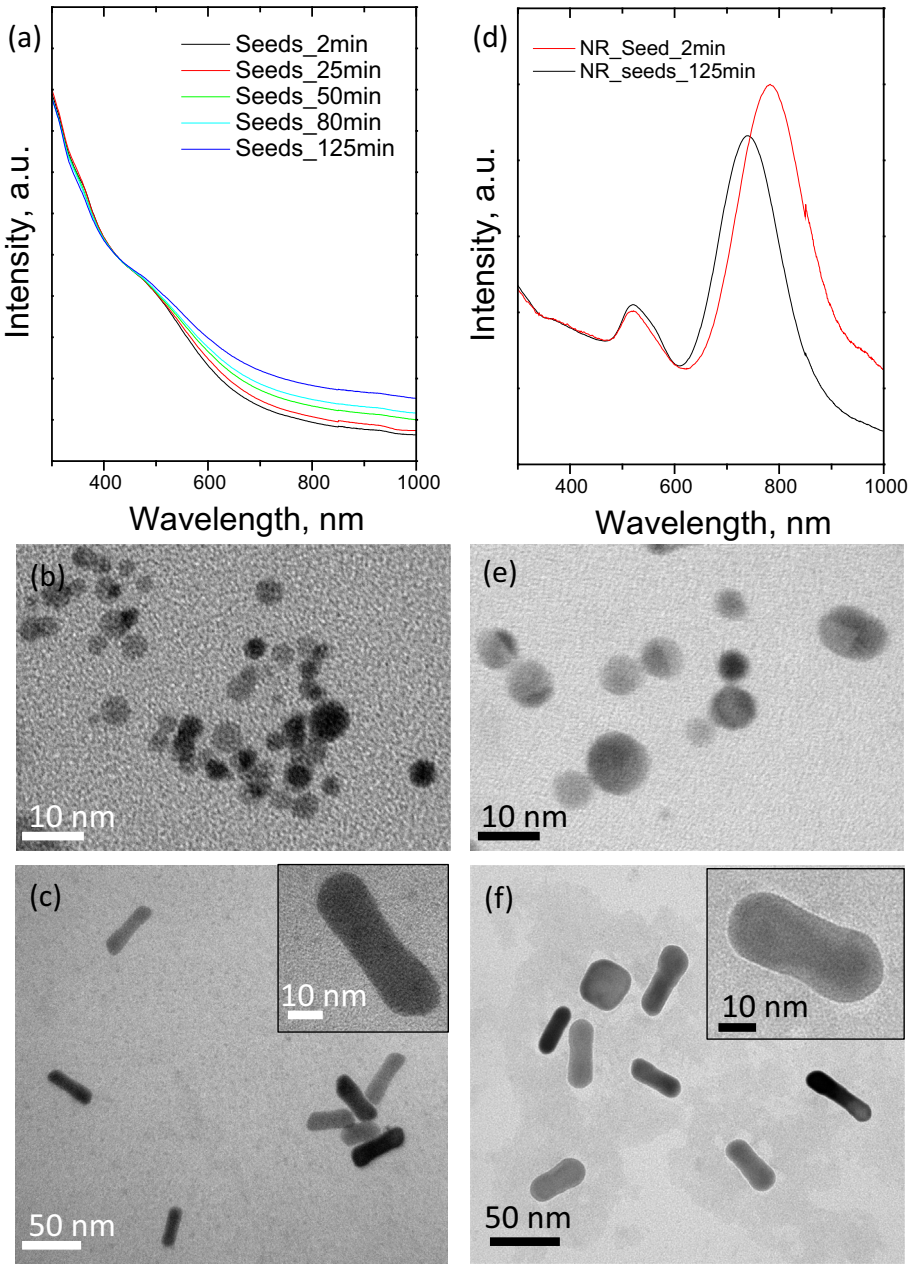

Fig. 2. Effect of aging time of the seeds on their size and on the characteristics of the resulting nanorods. (a) UVVIS extinction spectra of gold seeds at different aging times. TEM images corresponding to (b) seeds obtained after 2 min; (c) gold nanorods produced with 2 min aged seeds, (d) UVVIS extinction spectra of gold nanorods produced with gold seeds aged at 2 min and 125 min, respectively. TEM images corresponding to (e) gold seeds aged after 125 min; (f) gold nanorods produced with 125 min aged seeds.

system is operating at a low flow rate, as it is in our system, only small deviations from plug flow are expected due to the ability of radial diffusion to compensate a parabolic flow profile. In our case fouling was also avoided thanks to the material selection done for the construction of the microfluidic system. PTFE and PEEK are hydrophobic polymers and therefore, when using the aqueous precursor solution the surface wettability was reduced and consequently nanoparticle wall deposition was not observed.

As already mentioned, the microfluidic platform used also allows on-stream PEGylation of the continuously formed nanorods. The PEGylation process can be accomplished efficiently, with a considerable saving of PEG compared with traditional batch processes and without a significant effect on the physical or optical characteristics of the nanorods. Fig. 3 shows the UV–VIS extinction peaks of the PEGylated rods obtained in the experimental microfluidic set up using decreased amounts of PEG (up to 0,0113 μM) compared with the amounts used in the conventional batch reactor (1,13 μM). A slight blue shift was observed after PEGylation due to the change in the dielectric constant of the media [40]. The presence of PEG was also corroborated by TEM. The use of phosphotungstic acid to stain PEG allows visualization of the polymeric coating as a homogeneous (ca. 2.5 nm thick) halo around the gold nanorods (see Fig. 3c). The aspect ratio of the PEGylated nanorods (~5.1 ± 0.3) remained stable during at least one month of storage at room temperature, even with the lowest PEG/Au ratio used in the microfluidic reactor which corresponds to an amount 100 times lower than that used under batch-reaction conditions (see Fig. 3b). It is necessary to highlight that CTABr-capped gold nanorods suffer from morphological changes over time due to the loss of the CTABr coating, while replacement

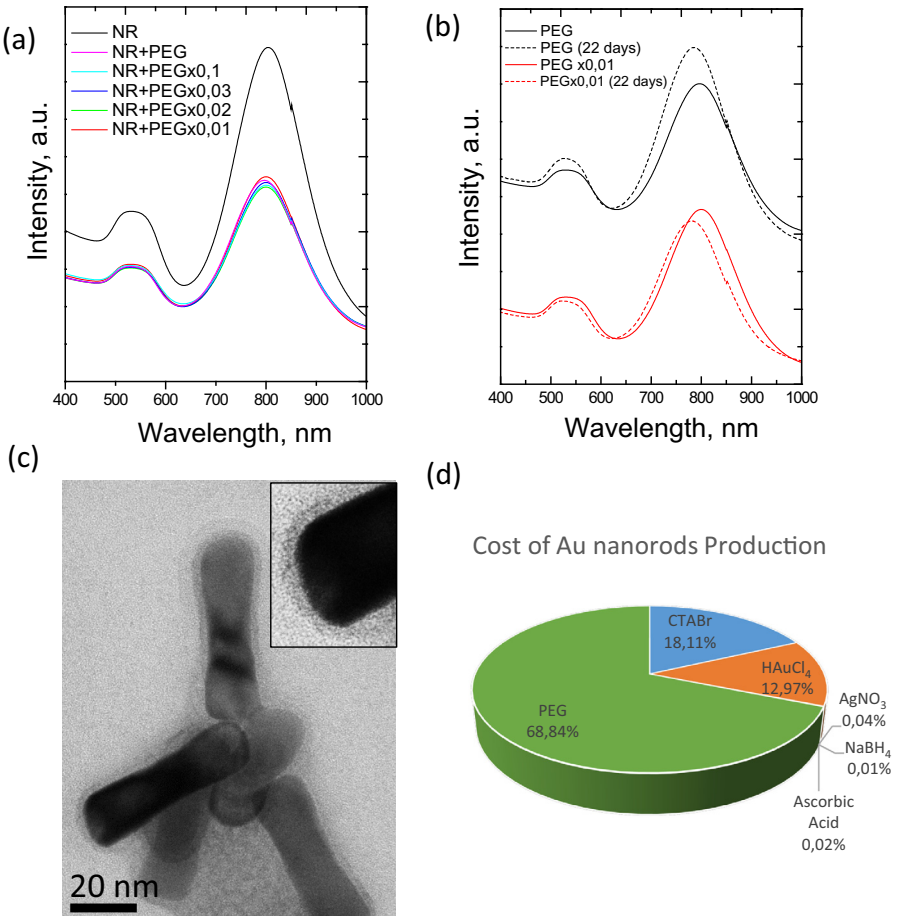

Fig. 3. On-stream PEGylation of gold nanorods. UVVIS extinction spectra of (a) PEGylated gold nanorods with decreased amounts of SH-PEG, (b) PEGylated gold nanorods after 22 days of production, (c) TEM images corresponding to PEGylated gold nanorods produced in the microfluidic continuous setup, with stained PEG coating. (d) Breakdown of cost of reagents for gold nanorods production at laboratory scale.

of CTABr by PEG produces stable nanorods [35], and therefore it is beneficial to functionalize the gold nanorods as soon as they are produced. Furthermore, if we make an analysis of the cost of reagents involved in producing the PEGylated nanorods at lab scale (using the amounts given in the experimental section for each specific chemical and the actual cost of materials from the suppliers), the cost PEG represents almost 69% of the total cost of materials (see Fig. 3d). It is important to point out that we just considered in that calculation the raw materials cost. Even though at industrial scale the cost ratios are likely to be different, a decrease of two orders of magnitude in the amount of one of the main contributors to the cost of raw materials implies a drastic cost reduction for the production of PEGylated gold nanorods.

Finally, since the flexibility of the microfluidic set up facilitates the study of operating variables we have used this characteristic to investigate the effect of replacing all or part of the Cl^- by Br^- in the reaction. Langille et al. [41] reported that the introduction of bromide or iodide slows down the rate of gold nanoparticle formation compared to the rate in the presence of chloride alone by lowering the reduction potential and solubility of the gold ion species in solution and by a stronger binding to the surface of the gold particles (the binding strength of the halides to gold increases in the order $Cl^- < Br^- < I^-$). Taking this into account we evaluated the influence of the introduction of bromide at different points in the microfluidic platform. Thus, keeping $HAuCl_4$ as gold precursor we have added 4-bromosalycilic acid to the feedstream containing $AgNO_3$ (inlet 1). This resulted in an increase of the gold nanorod aspect ratio (Fig. 4c) of from 5.3 to 6.1, with a clear effect on the UVVIS spectrum (Fig. 4a). Additional bromide could be introduced by replacing the gold precursor using $HAuBr_4$ instead of $HAuCl_4$ in inlet 2. In this case (Fig. 4b) the aspect ratio of the gold nanorods was very low (2.9) indicating that the presence chloride ions is required to obtain high aspect-ratio rods. Even in this case, the addition of 4-bromosalycilic acid produced a reshape and an increase in the final aspect ratio (6.8) of the resulting rods. As previously reported, the addition of chloride ions produces the most stable silver under-potential layer on the gold surface compared to other halides (bromide and iodide) [41]. The influence of the bromide ions was also corroborated in a batch reactor production mode. In this case, we observed that for nanorods obtained after 15 min of reaction time in a batch reactor the aspect ratio increased from 3.54 to 5.25 using a mixture (50:50) of $HAuCl_4$ and $HAuBr_4$ instead of $HAuCl_4$ alone. Fig. 5a shows a high-angle annular dark-field scanning transmission electron microscopy (HAADF-STEM) image taken from a sample produced with a mixture (50:50) of $HAuCl_4$ and $HAuBr_4$ in the microfluidic reactor. The high-resolution STEM (HR-STEM) image reveals that the gold nanorods are single-crystalline over the entire length. The observed lattice fringes of 0.23 can be assigned to the {1 1 1} planes of face-centered cubic (fcc) Au (Fig. 5b). The EDX analysis from a single Au nanorod shows a reduced amount of Ag atoms, but there were no traces of Cl and Br atoms. This means that the presence of those structure directing halide atoms has been reduced to values lower than the EDX detection limit (0.5 wt.%).

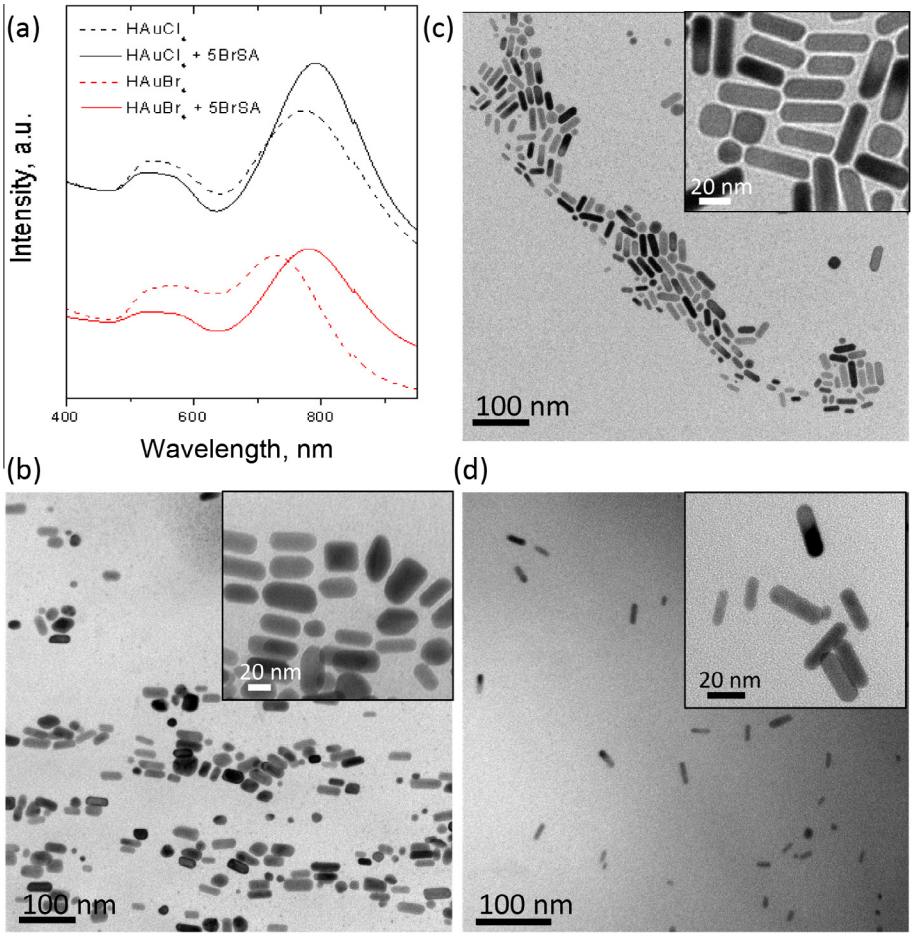

Fig. 4. Effect of bromide ions. (a) UVVIS extinction spectra of gold nanorods produced in the microfluidic system with different Au and Br sources, (b) TEM images corresponding to gold nanorods produced in the microreactor with $HAuCl_4$ and bromosalicylic acid, (c) with $HAuBr_4$, (d) using $HAuBr_4$ and bromosalicylic acid.

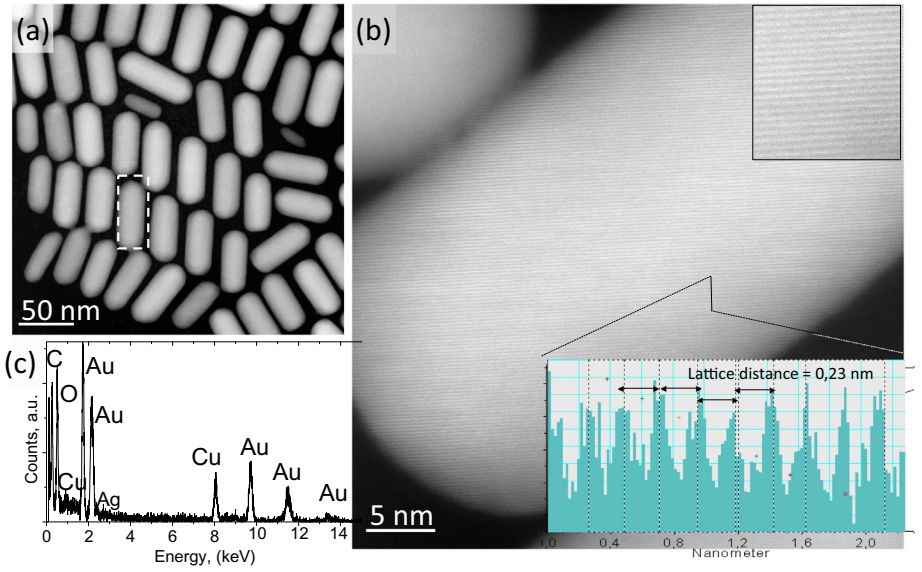

Fig. 5. Electron microscopy characterizations of the Au nanorods prepared in the microfluidic reactor with a mixture (50:50) of $HAuCl_4$ and $HAuBr_4$ as gold precursor and bromosalicylic acid (a) HAADF-STEM image of produced Au nanorods, (b) C_s-corrected STEM-HAADF image. Inset are a high-magnification STEM-HAADF image to show the lattice fringes and lattice fringe profile. (c) EDS analysis of a single gold nanorod from the area selected in (a).

4. Conclusions

A sequential multistep synthesis of PEGylated gold nanorods is possible using microfluidic reactors. This approach is highly effective towards the reduction of the PEG reagent used, and allows an excellent control of residence time in the seed forming and aging stages. This eliminates detrimental effects related to uncontrolled aging-related processes observed in the conventional synthesis of gold nanorods. The flexibility of the microfluidic system is also useful to fine-tune the presence of ionic modifiers (chloride and bromide ions) at different points in the synthesis process, allowing to tailor the aspect ratio of the final nanorods and consequently their optical properties.

Acknowledgments

Financial support from the EU thanks to the ERC Consolidator Grant program (ERC-2013-CoG-614715, NANOHEDONISM) and the People Program (CIG-Marie Curie Actions, REA grant agreement n° 321642) are gratefully acknowledged. CIBER-BBN is an initiative funded by the VI National R&D&i Plan 2008–2011, Iniciativa Ingenio 2010, Consolider Program, CIBER Actions and financed by the Instituto de Salud Carlos III (Spain) with assistance from the European Regional Development Fund.

References

[1] B.K. Park, S. Jeong, D. Kim, J. Moon, S. Lim, J.S. Kim, Synthesis and size control of monodisperse copper nanoparticles by polyol method, J. Colloid Interface Sci. 311 (2007) 417–424.
[2] J. Park, K.J. An, Y.S. Hwang, J.G. Park, H.J. Noh, J.Y. Kim, J.H. Park, N.M. Hwang, T. Hyeon, Ultra-large-scale syntheses of monodisperse nanocrystals, Nat. Mater. 3 (2004) 891–895.
[3] K.R. Brown, D.G. Walter, M.J. Natan, Seeding of colloidal Au nanoparticle solutions. 2. Improved control of particle size and shape, Chem. Mater. 12 (2000) 306–313.
[4] H. Nong-Moon, J. Jae-Soo, L. Dong-Kwon, Thermodynamics and kinetics in the synthesis of monodisperse nanoparticles, in: D.R. Morales-Rodriguez (Ed.), Thermodynamics – Fundamentals and Its Application in Science, InTech, 2012.
[5] W.R. Lee, M.G. Kim, J.R. Choi, J.I. Park, S.J. Ko, S.J. Oh, J. Cheon, Redox-transmetalation process as a generalized synthetic strategy for core–shell magnetic nanoparticles, J. Am. Chem. Soc. 127 (2005) 16090–16097.
[6] S.K. Sivaraman, S. Kumar, V. Santhanam, Room-temperature synthesis of gold nanoparticles – size-control by slow addition, Gold Bull. 43 (2010) 275–286.
[7] J. Polte, R. Kraehnert, M. Radtke, U. Reinholz, H. Riesemeier, A.F. Thunemann, F. Emmerling, New insights of the nucleation and growth process of gold nanoparticles via in situ coupling of SAXS and XANES, in: Xiv International Conference on Small-Angle Scattering (Sas09) 247, 2010.
[8] C.H. Chang, B.K. Paul, V.T. Remcho, S. Atre, J.E. Hutchison, Synthesis and post-processing of nanomaterials using microreaction technology, J. Nanopart. Res. 10 (2008) 965–980.
[9] X.Q. Chen, M. Arruebo, K.L. Yeung, Flow-synthesis of mesoporous silicas and their use in the preparation of magnetic catalysts for Knoevenagel condensation reactions, Catal. Today 204 (2013) 140–147.
[10] A. Toyota, H. Nakamura, H. Ozono, K. Yamashita, M. Uehara, H. Maeda, Combinatorial synthesis of CdSe nanoparticles using microreactors, J. Phys. Chem. C 114 (2010) 7527–7534.
[11] J.M. Lim, A. Swami, L.M. Gilson, S. Chopra, S. Choi, J. Wu, R. Langer, R. Karnik, O. C. Farokhzad, Ultra-high throughput synthesis of nanoparticles with homogeneous size distribution using a coaxial turbulent jet mixer, ACS Nano 8 (2014) 6056–6065.
[12] K.I. Min, D.J. Im, H.J. Lee, D.P. Kim, Three-dimensional flash flow microreactor for scale-up production of monodisperse PEG-PLGA nanoparticles, Lab Chip 14 (2014) 3987–3992.
[13] S.E. Lohse, J.R. Eller, S.T. Sivapalan, M.R. Plews, C.J. Murphy, A simple millifluidic benchtop reactor system for the high-throughput synthesis and functionalization of gold nanoparticles with different sizes and shapes, ACS Nano 7 (2013) 4135–4150.
[14] S. Krishnadasan, R.J.C. Brown, A.J. deMello, J.C. deMello, Intelligent routes to the controlled synthesis of nanoparticles, Lab Chip 7 (2007) 1434–1441.
[15] L. Gomez, V. Sebastian, S. Irusta, A. Ibarra, M. Arruebo, J. Santamaria, Scaled-up production of plasmonic nanoparticles using microfluidics: from metal precursors to functionalized and sterilized nanoparticles, Lab Chip 14 (2014) 325–332.
[16] A. Gunther, S.A. Khan, M. Thalmann, F. Trachsel, K.F. Jensen, Transport and reaction in microscale segmented gas–liquid flow, Lab Chip 4 (2004) 278–286.
[17] S.A. Khan, A. Gunther, M.A. Schmidt, K.F. Jensen, Microfluidic synthesis of colloidal silica, Langmuir 20 (2004) 8604–8611.
[18] H. Nakamura, Y. Yamaguchi, M. Miyazaki, H. Maeda, M. Uehara, P. Mulvaney, Preparation of CdSe nanocrystals in a micro-flow-reactor, Chem. Commun. (2002) 2844–2845.
[19] B.K.H. Yen, A. Gunther, M.A. Schmidt, K.F. Jensen, M.G. Bawendi, A microfabricated gas–liquid segmented flow reactor for high-temperature synthesis: the case of CdSe quantum dots, Angew. Chem. Int. Ed. 44 (2005) 5447–5451.
[20] Z.L. Xue, A.D. Terepka, Y. Hong, Synthesis of silver nanoparticles in a continuous flow tubular microreactor, Nano Lett. 4 (2004) 2227–2232.
[21] W.B. Lee, C.H. Weng, F.Y. Cheng, C.S. Yeh, H.Y. Lei, G.B. Lee, Biomedical microdevices synthesis of iron oxide nanoparticles using a microfluidic system, Biomed. Microdevices 11 (2009) 161–171.
[22] M. Schuch, G.A. Gross, J.M. Kohler, Formation and fluorimetric characterization of micelles in a micro-flow through system with static micro mixer, Sensors-Basel 7 (2007) 2499–2509.
[23] I.V. Zhigaltsev, N. Belliveau, I. Hafez, A.K.K. Leung, J. Huft, C. Hansen, P.R. Cullis, Bottom-up design and synthesis of limit size lipid nanoparticle systems with aqueous and triglyceride cores using millisecond microfluidic mixing, Langmuir 28 (2012) 3633–3640.
[24] C.T. Lo, A. Jahn, L.E. Locascio, W.N. Vreeland, Controlled self-assembly of monodisperse niosomes by microfluidic hydrodynamic focusing, Langmuir 26 (2010) 8559–8566.
[25] M. Faustini, J. Kim, G.Y. Jeong, J.Y. Kim, H.R. Moon, W.S. Ahn, D.P. Kim, Microfluidic approach toward continuous and ultrafast synthesis of metal-organic framework crystals and hetero structures in confined microdroplets, J. Am. Chem. Soc. 135 (2013) 14619–14626.
[26] J. Boleininger, A. Kurz, V. Reuss, C. Sonnichsen, Microfluidic continuous flow synthesis of rod-shaped gold and silver nanocrystals, Phys. Chem. Chem. Phys. 8 (2006) 3824–3827.
[27] J.M. Kohler, H. Romanus, U. Hubner, J. Wagner, Formation of star-like and core–shell AuAg nanoparticles during two- and three-step preparation in batch and in microfluidic systems, J. Nanomater. (2007).
[28] C.J. Murphy, T.K. San, A.M. Gole, C.J. Orendorff, J.X. Gao, L. Gou, S.E. Hunyadi, T. Li, Anisotropic metal nanoparticles: Synthesis, assembly, and optical applications, J. Phys. Chem. B 109 (2005) 13857–13870.
[29] X.L. Xu, Y.Y. Zhao, X.D. Xue, S.D. Huo, F. Chen, G.Z. Zou, X.J. Liang, Seedless synthesis of high aspect ratio gold nanorods with high yield, J. Mater. Chem. A 2 (2014) 3528–3535.
[30] B. Nikoobakht, M.A. El-Sayed, Preparation and growth mechanism of gold nanorods (NRs) using seed-mediated growth method, Chem. Mater. 15 (2003) 1957–1962.
[31] J.E. Millstone, W. Wei, M.R. Jones, H.J. Yoo, C.A. Mirkin, Iodide ions control seed-mediated growth of anisotropic gold nanoparticles, Nano Lett. 8 (2008) 2526–2529.
[32] C.J. Murphy, L.B. Thompson, A.M. Alkilany, P.N. Sisco, S.P. Boulos, S.T. Sivapalan, J.A. Yang, D.J. Chernak, J.Y. Huang, The many faces of gold nanorods, J. Phys. Chem. Lett. 1 (2010) 2867–2875.
[33] S. Duraiswamy, S.A. Khan, Dual-stage continuous-flow seedless microfluidic synthesis of anisotropic gold nanocrystals, Part. Part. Syst. Charact. 31 (2014) 429–432.
[34] V. Sebastian, S.K. Lee, C. Zhou, M.F. Kraus, J.G. Fujimoto, K.F. Jensen, One-step continuous synthesis of biocompatible gold nanorods for optical coherence tomography, Chem. Commun. 48 (2012) 6654–6656.
[35] L. Gomez, V. Cebrian, F. Martin-Saavedra, M. Arruebo, N. Vilaboa, J. Santamaria, Stability and biocompatibility of photothermal gold nanorods after lyophilization and sterilization, Mater. Res. Bull. 48 (2013) 4051–4057.
[36] A. Gole, C.J. Murphy, Seed-mediated synthesis of gold nanorods: role of the size and nature of the seed, Chem. Mater. 16 (2004) 3633–3640.
[37] G. von Maltzahn, J.H. Park, A. Agrawal, N.K. Bandaru, S.K. Das, M.J. Sailor, S.N. Bhatia, Computationally guided photothermal tumor therapy using long-circulating gold nanorod antennas, Cancer Res. 69 (2009) 3892–3900.
[38] G. Schmid, B. Corain, Nanoparticulated gold: syntheses, structures, electronics, and reactivities, Eur. J. Inorg. Chem. (2003) 3081–3098.
[39] M.M. Alvarez, J.T. Khoury, T.G. Schaaff, M.N. Shafigullin, I. Vezmar, R.L. Whetten, Optical absorption spectra of nanocrystal gold molecules, J. Phys. Chem. B 101 (1997) 3706–3712.
[40] A.M. Goodman, Y. Cao, C. Urban, O. Neumann, C. Ayala-Orozco, M.W. Knight, A. Joshi, P. Nordlander, N.J. Halas, The surprising in vivo instability of near-IR-absorbing hollow Au–Ag nanoshells, ACS Nano 8 (2014) 3222–3231.
[41] M.R. Langille, M.L. Personick, J. Zhang, C.A. Mirkin, Defining rules for the shape evolution of gold nanoparticles, J. Am. Chem. Soc. 134 (2012) 14542–14554.